

CAMEL: Physically Inspired Crosstalk-Aware Mapping and gate scheduling for Frequency-Tunable Quantum Chips

Bin-Han Lu^{*†}, Peng Wang^{*†}, Zhao-Yun Chen[‡], Huan-Yu Liu^{*†}, Tai-Ping Sun^{*†}, Peng Duan^{*†}, Yu-Chun Wu^{*†‡}, Guo-Ping Guo^{*†‡}

* Key Laboratory of Quantum Information Chinese Academy of Sciences, School of Physics, University of Science and Technology of China, Hefei, Anhui, 230026, P. R. China

† CAS Center For Excellence in Quantum Information and Quantum Physics, University of Science and Technology of China, Hefei, Anhui, 230026, P. R. China

‡ Institute of Artificial Intelligence, Hefei Comprehensive National Science Center, Hefei, Anhui, 230026, P. R. China

Abstract—Crosstalk poses a significant challenge in quantum computing, particularly when quantum gates are executed in parallel, as qubit frequency resonance can lead to residual coupling and reduced gate fidelity. Current solutions struggle to mitigate both crosstalk and decoherence during parallel two-qubit gate operations on frequency-tunable quantum chips. To address this, we propose a crosstalk-aware mapping and gate scheduling (CAMEL) approach, designed to mitigate crosstalk and suppress decoherence by leveraging the tunable coupler’s physical properties and incorporating a pulse compensation technique. CAMEL operates within a two-step compilation framework: first, a qubit mapping strategy that considers both crosstalk and decoherence; and second, a gate timing scheduling method that prioritizes the execution of the largest possible set of crosstalk-free parallel gates, reducing overall circuit execution time. Evaluation results demonstrate CAMEL’s superior ability to mitigate crosstalk compared to crosstalk-agnostic methods, while successfully suppressing decoherence where other approaches fail. Additionally, CAMEL exhibits better performance than dynamic-frequency-aware techniques, particularly in low-complexity hardware environments.

I. INTRODUCTION

Quantum computing has advanced into the noisy intermediate-scale quantum (NISQ) era, characterized by chips containing dozens to hundreds of qubits [1]. Superconducting qubits are among the leading technologies for NISQ devices [2], but despite their potential, they face significant challenges from two primary sources of noise: decoherence and crosstalk. Decoherence, caused by environmental interactions, gradually erodes quantum coherence over time [3]–[5]. Meanwhile, crosstalk, resulting from unintended qubit coupling, becomes problematic when qubit frequencies approach resonance, leading to increased errors during the parallel execution of multiple quantum gates [6]. These noise-related issues greatly affect the performance and reliability of NISQ systems.

Effective noise suppression strategies are essential [7] to ensure quantum computations are completed before significant decoherence occurs. Current solutions [8], [9] focus on

optimizing qubit mapping to reduce execution time. However, crosstalk complicates this, as increased parallelism can amplify errors. Simply serializing gate execution to mitigate crosstalk would negate the time-saving benefits of optimized mapping. Therefore, approaches that address both decoherence and crosstalk while maintaining parallelism are critical for fully realizing the potential of NISQ quantum processors.

To mitigate crosstalk, software-level solutions often involve serializing the execution of parallel gates significantly impacted by crosstalk. A scheduling approach has been proposed that accounts for both crosstalk and decoherence by employing a multi-objective function [10]. Another solution introduces gate scheduling based on graph coloring to reduce crosstalk during parallel gate execution [11]. While these approaches address crosstalk by serializing affected gates, this increases the overall execution time of quantum circuits, thereby raising the risk of decoherence errors.

In addition to software solutions, researchers are exploring hardware-level methods to reduce crosstalk. These efforts include optimizing qubit architecture [12], [13], using microwave control for qubits and couplers [14], [15], and adjusting tunable couplers to reach a minimum ZZ crosstalk frequency [16], [17]. These hardware approaches are particularly effective at mitigating crosstalk in single-qubit gates.

In frequency-tunable superconducting qubits [18], qubit frequencies shift from their single-qubit idle frequency to a two-qubit interaction frequency during the execution of two-qubit gates. If the frequency of a neighboring spectator qubit is near resonance with the gate qubit, unwanted population swap can occur, making previous hardware solutions ineffective. This issue is referred to as frequency crowding. To address this, a frequency configuration technique was proposed to reduce crosstalk by avoiding near-resonance scenarios [19]. However, as the scale of chips increases and arbitrary parallel gate execution becomes necessary, the exponential growth of parallel two-qubit gate scenarios renders frequency configuration impractical. As an alternative, Ding et al. [20] proposed a dynamic frequency configuration approach. However, this

method does not include the calibration of gate pulse parameters, which involves repeatedly executing gates and fine-tuning control parameters to minimize errors [21]. Calibration must be completed prior to circuit execution [22]. Implementing real-time calibration for the dynamic frequency configuration strategy, as required by [20], is not feasible during circuit execution.

Building on the physical properties of frequency-tunable superconducting qubits, we introduce a scalable approach: **crosstalk-aware mapping and gate scheduling (CAMEL)**. This approach is designed to mitigate both crosstalk and decoherence in frequency-tunable systems. We have demonstrated that crosstalk errors in two-qubit gates on frequency-tunable quantum chips stem from population swap between gate qubits and spectator qubits. Furthermore, we identified a population swap cutoff frequency in the spectator coupler, indicating that near-resonance effects between two-qubit gates and spectator qubits can still be mitigated by applying compensation pulses to the spectator coupler, even after frequency configuration has been completed.

To further extend crosstalk mitigation beyond local windows, we introduce a crosstalk-aware mapping strategy along with a gate scheduling method based on the maximum independent set problem, optimizing execution time while effectively reducing crosstalk across the chip. To address the challenge posed by the growing number of parallel gate execution scenarios, we partition the chip into local windows. Compared to the dynamic frequency configuration approach proposed in [20], CAMEL completes calibration prior to quantum program execution, as the number of windows and qubits remains consistent.

Our key contributions are as follows:

- A pulse compensation method was introduced to mitigate two-qubit gate population swap crosstalk in frequency-tunable superconducting qubits, and its effectiveness was demonstrated through both theoretical analysis and simulations.
- A crosstalk-aware qubit mapping and gate scheduling approach was developed, expanding the local crosstalk suppression capability of the compensation pulse across the entire chip.
- The evaluation was performed using widely adopted benchmarks for the current NISQ era, including cross-entropy benchmarking circuits [23], all of which produced satisfactory results.

II. PRELIMINARIES

A. Fundamental information for quantum computing

A qubit, the fundamental unit of quantum information, is described by a superposition $|\psi\rangle = \alpha|0\rangle + \beta|1\rangle$, where $|\alpha|^2 + |\beta|^2 = 1$. A quantum computer with n qubits has a superposition over 2^n basis states. Quantum computations are executed with quantum gates, which can be decomposed into single or two-qubit gates. Quantum circuits, consisting of input qubits, quantum gates, measurements, and classical registers, serve as the building blocks of quantum programs.

The circuit can also be modeled as a directed acyclic graph (DAG) $\mathcal{D}(\mathbf{q}, \mathbf{g}, \mathbf{e})$ [24].

The coupling structure of a quantum chip is represented as a graph $\mathcal{G}(\mathbf{Q}, \mathbf{E})$, where \mathbf{Q} denotes the physical qubits and \mathbf{E} represents the couplers. Two-qubit gates (such as CZ gate) between $q_i \in \mathbf{Q}$ and $q_j \in \mathbf{Q}$ can be executed only when $(q_i, q_j) \in \mathbf{E}$.

Quantum systems are highly sensitive to environmental noise, which can induce decoherence [4]. The probability of qubit decoherence increases exponentially over time, governed by $P(t) = 1 - \exp\left(-\frac{t}{T_i}\right)$, where T_i represents the decoherence time. There are two types of decoherence times: the relaxation time T_1 , which represents the transition rate from the excited state to the ground state, and the dephasing time T_2 , which represents the rate of phase information loss. To prevent errors, a quantum circuit must complete its execution within the decoherence time.

B. Superconducting quantum computing hardware

1) *Tunable qubit*: The qubit frequency corresponds to the energy transition between the ground state $|0\rangle$ and the excited state $|1\rangle$, represented by $\omega = \omega_{01} = E_1 - E_0$, as shown in Fig. 1(a). The anharmonicity parameter η ensures that $\omega_{12} = \omega_{01} + \eta$, detuning the second excited state $|2\rangle$ from ω_{01} to prevent unwanted transitions. In frequency-tunable superconducting qubits (or tunable qubits), the frequency is controlled by an external magnetic flux Φ , with the frequency spectrum shown in Fig. 1(b). The coherence time T_1 decreases near two-level system (TLS) defect points [25], while T_2 is proportional to $d\omega/d\Phi$ [3]. To achieve a long T_i , the qubit frequency must be positioned where $d\omega/d\Phi$ is minimal and away from TLS defect points, constraining the available frequency range.

2) *Tunable coupler* [26]: The tunable coupler is a promising technological approach for superconducting chips, relying on a specialized structure to control the coupling strength between qubits. This technology has seen widespread adoption [27], [28] and has been employed in important experiments, including those demonstrating quantum supremacy [23] and quantum error correction codes [29], [30]. These applications underscore the tunable coupler's significant potential for scaling up quantum computers.

In Fig. 1(c), the effective coupling strength \tilde{g}_{12} reaches a minimum, signifying the elimination of crosstalk. In Fig. 1(d), the frequencies of Q_1 and Q_2 satisfy $\omega_1 + \eta_1 = \omega_2$ [2], causing the states $|11\rangle$ and $|02\rangle$ to become resonant. Simultaneously, the frequency of c_{12} must be tuned to a lower point with larger \tilde{g}_{12} , as depicted in Fig. 1(c), to ensure fast gate execution. Subsequently, after $t_g = \pi/\tilde{g}_{12}$, the state $|11\rangle$ undergoes a phase shift: $|11\rangle \xrightarrow{e^{i\pi/2}} i|02\rangle \xrightarrow{e^{i\pi}} -|11\rangle$, thus realizing the CZ gate.

C. Gate pulse calibration [21]

Quantum gates are implemented by applying time-dependent pulses to qubits, represented by the function $f(t; \alpha)$, where α denotes the control parameters. Before

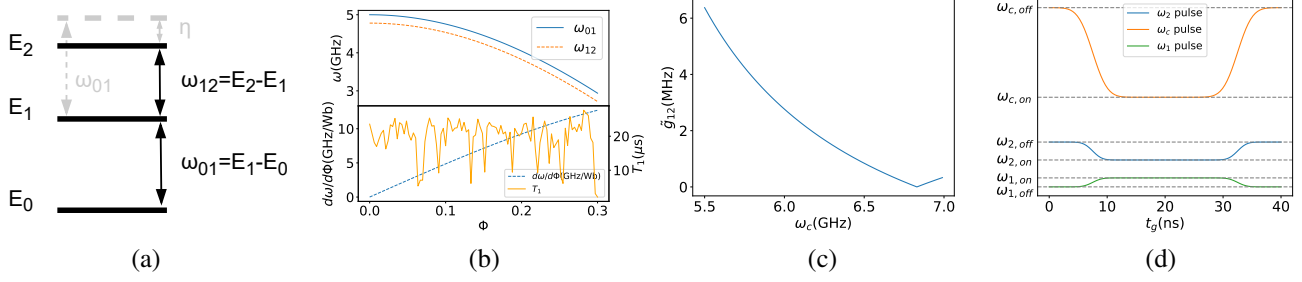


Fig. 1: (a) The energy level diagram for superconducting qubits. (b) The frequency spectrum for tunable qubits. When the frequency is close to the maximum point, $d\omega/d\Phi$ is small. T_1 is reduced at TLS defect points. (c) The relationship between \tilde{g}_{12} and the coupler frequency. A specific coupler frequency exists at which \tilde{g}_{12} reaches zero. As the coupler frequency decreases, the magnitude of $|\tilde{g}_{12}|$ increases. (d) The dynamic gate pulse applied to qubits Q_1 and Q_2 , as well as the coupler c_{12} between them. The qubit frequencies ω_i shift from $\omega_{i,\text{off}}$ to interaction frequency $\omega_{i,\text{on}}$, ensuring the resonant condition $\omega_1 + \eta_1 = \omega_2$ is met. Additionally, the coupler frequency decreases from $\omega_{c,\text{off}}$ to $\omega_{c,\text{on}}$ to enlarge \tilde{g}_{12} .

executing a quantum circuit, the gates undergo calibration to determine the optimal parameters α^* that maximize the fidelity. This iterative process requires multiple executions and measurements, making it impractical to perform during circuit execution.

D. Crosstalk error

1) *Single-qubit gate crosstalk*: When qubit frequencies are close to those of neighboring qubits, crosstalk can occur, resulting in unwanted transitions such as $|01\rangle \leftrightarrow |10\rangle$ and $|11\rangle \leftrightarrow |02\rangle$ [31]. Additionally, the microwave signal applied to a single-qubit gate on qubit Q_i can affect non-target qubit Q_j [32]. To minimize crosstalk, qubits should be kept in a far-detuned regime, imposing constraints on the allowable frequency range.

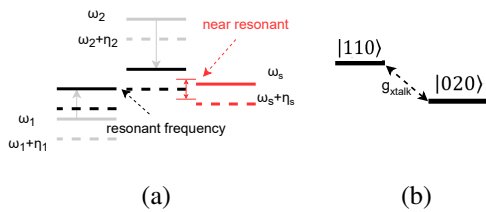


Fig. 2: (a) The energy level model for the CZ gate qubits Q_1 and Q_2 , alongside the spectator qubit Q_s . ω_1 and $\omega_2 + \eta_2$ denote interaction frequencies. The frequency ω_s of the spectator qubit is close to the resonant frequency. (b) The crosstalk model considers the qubits in the order $|Q_s Q_2 Q_1\rangle$, where Q_1 and Q_2 are interacting in state $|020\rangle$. If E_{110} resonates with E_{020} , population swap from $|020\rangle$ to $|110\rangle$ will occur.

When neighboring qubit frequencies are in the far-detuned regime, there is no population swap between them, and the coupling Hamiltonian is given by $H/\hbar = E_{\tilde{n}}|\tilde{n}\rangle$. Here, $E_{\tilde{n}}$ represents the energy levels of the dressed states, and the energy shift $\xi = E_{\tilde{11}} - E_{\tilde{01}} - E_{\tilde{10}} + E_{\tilde{00}}$ is referred to as ZZ coupling [33]. Adjusting the coupler frequency to minimize the ZZ coupling effectively suppresses this type of crosstalk.

2) *Two-qubit gate crosstalk*: There are various scenarios of frequency crowding between the two-qubit gates and the spectator qubit. We take one of these scenarios as an example to explain in detail the physical mechanism of the population swap from the gate state to the excited state of the spectator qubit. Consider the model in Fig. 2(a), where qubits Q_1 and Q_2 serve as the CZ gate qubits, with their frequencies tuned to resonance, and Q_s acts as a spectator qubit connected to Q_2 . The energy levels satisfy $E_{020} = E_{011}$, which correspond to the CZ gate level. Additionally, $E_{011} = \omega_1 + \omega_2$ and $E_{110} = \omega_s + \omega_2$. To prevent crosstalk, it is crucial to ensure that E_{110} is sufficiently far from E_{020} during the execution of the CZ gate. Otherwise, a population swap from $|020\rangle$ to $|110\rangle$ will occur Fig. 2(b).

3) *Frequency crowding*: The constraints discussed in the previous sections reduce the available frequency range for qubits. Moreover, straying too far from the optimal “sweet point” (around 500 MHz) significantly shortens the decoherence time, meaning the qubit frequency must stay within the range $(\omega_{\text{max}} - 500\text{MHz}, \omega_{\text{max}})$ to maintain coherence [34]. On a square periodic chip, each qubit has four nearest neighbors and eight next-nearest neighbors, while each two-qubit gate is affected by six spectator qubits and up to 10 potentially crosstalking parallel gates. Each near-resonance region spans over 20 MHz, further limiting the effective frequency range, which is known as “frequency crowding”. If two parallel gates experience crosstalk due to qubit frequency crowding, they must be executed sequentially. This adjustment, however, increases circuit runtime and raises the risk of decoherence.

III. USING COMPENSATION PULSE TO MITIGATE CROSSTALK

A. Compensation pulse

In Section II-D2, we hypothesize that the crosstalk is caused by the population swap from the gate state $|020\rangle$ to the spectator qubit’s excited state $|110\rangle$. To investigate this, we conducted simulations by varying the frequency of the spectator qubit. In Fig. 3(a), we observe that population swap and error increase simultaneously when E_{110} approaches

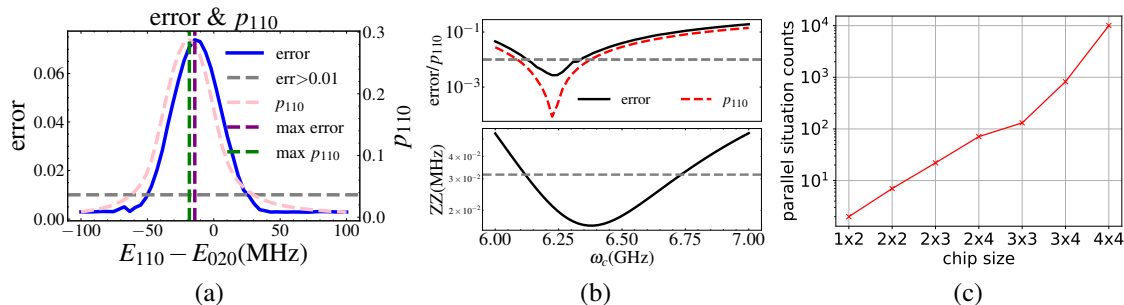


Fig. 3: (a) The population swap from $|020\rangle$ to $|110\rangle$ and gate errors when the spectator qubit is at different frequencies. The horizontal axis represents the energy difference between $|110\rangle$ and $|020\rangle$. As the frequency of the spectator qubit varies, both population swap and gate errors clearly increase simultaneously. In the 100 MHz range, gate errors exceed 0.01, indicated by the grey line. (b) The relationship between CZ gate error, population swap p_{110} and ZZ coupling on coupler frequency, with the qubit order as $|Q_s Q_2 Q_1\rangle$. (c) The diagram illustrates how the number of parallel situations for two-qubit gates changes with the scale of the $M \times N$ chip.

resonance with E_{020} . If this entire range above the grey line is treated as a frequency exclusion zone, the frequency constraints on qubits will become too restrictive, resulting in significant frequency crowding. Next, we will demonstrate that this population swap can be suppressed by adjusting the coupler frequency.

As a result of the unwanted coupling between of Q_2 and Q_s , the system Hamiltonian is expressed as follows:

$$H/\hbar = \begin{pmatrix} E_{020}/\hbar & g_{\text{xtalk}} \\ g_{\text{xtalk}} & E_{110}/\hbar \end{pmatrix}. \quad (1)$$

The first energy level corresponds to $|020\rangle$, and the second energy level represents $|110\rangle$. The term g_{xtalk} denotes the coupling strength between $|020\rangle$ and $|110\rangle$, which is a function of ω_1 , ω_2 , ω_s , and ω_c [35]. During the execution of single-qubit gates, the detuning between Q_s and Q_2 , as well as between Q_2 and Q_1 , is large, and the ω_c is set at the ZZ minimum, resulting in a negligible g_{xtalk} . However, when executing two-qubit gates on Q_1 and Q_2 , the qubits are tuned to a resonance frequency, and the coupler moves away from the ZZ minimum. This change reduces the detuning between the qubits and results in a non-zero g_{xtalk} . Zajac et al. [36] proposed a method using compensation pulses to mitigate stray coupling in fixed-frequency qubits. Through simulations, we found that in a frequency-tunable system, we can similarly adjust the ω_c with compensation pulses to suppress the population swap from the gate state $|020\rangle$ to the state $|110\rangle$.

In the simulation, we set $E_{110} = E_{020}$, shifting the ω_c to calculate the population swap and error, comparing them with the ZZ coupling strength at the idle frequency. In Fig. 3(b), the frequency corresponding to the minimum error is not the same as the ZZ minimum frequency. Additionally, the minimum population swap between $|020\rangle$ and $|110\rangle$ coincides with the minimum error. Therefore, it is possible to readjust the spectator coupler to ensure that g_{xtalk} is small, thus protecting the fidelity of the two-qubit gate from the crosstalk of spectator qubit Q_s .

Hence, we propose a pulse compensation approach for the population swap of parallel quantum gates. If a frequency

crowding occurs between the two-qubit gate and spectator qubits, we dynamically adjust the spectator coupler's frequency. This adjustment shifts from the ZZ coupling minimum to the population swap minimum. Similar to gate calibration, this compensation pulse calibration must be done before circuit execution. By using compensation pulses, even when the gate qubits are resonant with the frequency of spectator qubits, population swap can be avoided. This approach partially mitigates frequency crowding, reduces the constraints on the frequency range, and lessens the difficulty of subsequent quantum circuit mapping and scheduling.

B. Limitation of compensation pulse approach

Although compensation pulses can mitigate crosstalk errors on a quantum chip, applying them across the entire chip poses a computationally hard problem. In any given quantum circuit, a large number of parallel configurations of two-qubit gates can occur within a single circuit layer. Identifying all possible parallel configurations of two-dimensional two-qubit gates on the chip is equivalent to solving an independent set problem, and the number of independent sets in a graph generally increases exponentially with the size of the graph [37], [38]. For a square periodic planar chip structure of size $M \times N$, we calculate the growth in the number of independent sets as M and N increase, as shown in Fig. 3(c). Consequently, the compensation pulse cannot achieve global crosstalk suppression across the chip.

The limitation of the compensation pulse technique forces us to focus on mitigating crosstalk in a smaller region of the chip, referred to as a windowed compensation pulse. Developing an effective way to integrate this windowed compensation pulse into a compilation scheme is crucial for reducing quantum circuit errors on a broader scale.

IV. QUBIT MAPPING & GATE SCHEDULING

Decoherence requires minimizing the execution time of a quantum circuit, while frequency crowding demands that parallel quantum gates be executed sequentially, which in

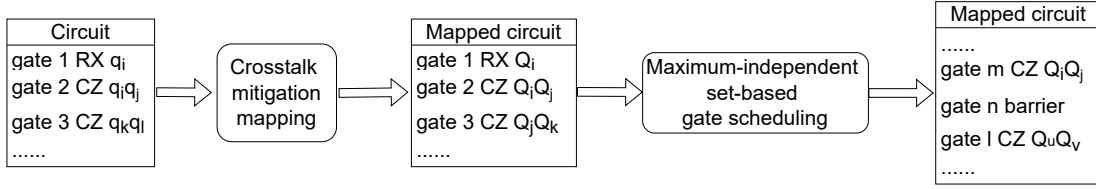


Fig. 4: The algorithm consists of two main steps. Firstly, given a quantum circuit, it undergoes crosstalk-aware mapping to produce a mapped circuit, where logical qubits q are mapped to physical qubits Q . Secondly, gate scheduling based on the maximum independent set is applied, with barriers inserted at appropriate positions to mitigate crosstalk.

turn increases the overall execution time. Additionally, the compensation pulse can only mitigate crosstalk locally. Given these constraints, it is crucial to develop an optimal qubit mapping and gate scheduling strategy that extends the local crosstalk mitigation capabilities of the compensation pulse across the entire chip. In this section, we systematically introduce our CAMEL compilation approach, detailing each step to demonstrate how our design mitigates both crosstalk and decoherence. To provide an overview, the algorithmic flow of CAMEL is illustrated in Fig. 4.

A. Basic elements

1) *Distance matrix*: Given a coupling graph $\mathcal{G}(\mathbf{Q}, \mathbf{E})$, we define a distance matrix $D(\cdot, \cdot)$ where each element represents the shortest path between qubit-pairs.

2) *Top layer*: The top layer, denoted as F , consists of pending gates that do not have any unexecuted predecessors within the DAG. For instance, $g(q_i, q_j)$ is appropriate to be placed in the set F once all preceding gates on q_i and q_j have been executed.

3) *Gate duration*: Given that the execution time of gate g is t_g , if it starts executing at time $g.t$, it finishes execution at $g.t + t_g$.

4) *Swap gate*: Suppose a mapping at time t_1 is denoted by π_1 . If we insert a swap gate s , we will obtain a new mapping π_2 $\pi_1(q_1) = \pi_2(q_2) \cap \pi_1(q_2) = \pi_2(q_1) \cap \pi_1(q) = \pi_2(q), \forall q \neq q_1, q_2$ at $t_2 \leftarrow t_1 + t_s$. We define all possible swap gate as a set \mathcal{S} .

B. Constraint

To achieve the highest fidelity, calibration of quantum gate parameters is crucial [39]. In addition, we also need to calibrate the compensation pulses for the spectator couplers neighboring the gate qubits. Initially, all the spectator qubits surrounding the gate qubits are at idle frequencies.

When executing multiple CZ gates in parallel, the frequency configuration of neighboring CZ gates should ideally avoid frequency crowding. However, as mentioned in Section III-B, the count of parallel situations increases exponentially with the chip size. Frequency configuration, gate, and compensation pulse calibration for all situations are impractical. In other words, frequency crowding is inevitable.

An alternative approach involves calibrating every $m \times n$ ($m, n < N$) qubit window on the chip, as illustrated in Fig. 5. We perform a frequency configuration and parameter calibration considering every possible parallel scenario within

the window. For an $M \times N$ chip, the number of windows, $(M - m + 1)(N - n + 1)$, is of the same order of magnitude as the number of qubits. Configuring frequencies and calibrating gate and compensation pulse parameters for all scenarios before circuit execution is feasible. When scheduling the execution of CZ gates, they must be mapped to physical qubits within the same window or non-adjacent windows to avoid unintended frequency crowding.

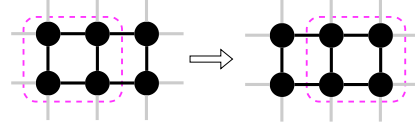


Fig. 5: The qubits and couplers within the $m \times n, m = n = 2$ window are calibrated to enable parallel execution of any CZ gates. By sliding and calibrating this window across the chip, any gates in $m \times n$ window at any position on the chip can be executed parallelly.

Building upon this concept, the parallel constraint arises from the maximum window size of $m \times n$. If a set of gates \mathbf{g} temporally overlaps, expressed as:

$$\forall g_i, g_j \in \mathbf{g}, (g_i.t, g_i.t + t_{g_i}) \cap (g_j.t, g_j.t + t_{g_j}) \neq \emptyset. \quad (2)$$

Gate qubits should be mapped to physical qubits within non-adjacent windows.

Suppose the maximum allowed window size is $m \times n$, with the graph diameter of the window being $m + n - 2$. Given a mapping π and a list of pending gates \mathbf{g} , we define a subset $\mathbf{Q}_g = \{\pi(q) | \forall g \in \mathbf{g}, q \in g.q\}$, and obtain an algorithm subgraph \mathcal{G}_g of \mathcal{G} containing only \mathbf{Q}_g . For a maximum window with size $m \times n$, the constraint can be expressed as follows:

$$\max(d_g) \leq m + n - 2, \quad (3)$$

where d_g represents the graph diameter of all connected subgraphs of \mathcal{G}_g . These windows can locally mitigate crosstalk. The window size depends on the frequency configuration and pulse parameter calibration scale that the chip control system can simultaneously achieve, as described in Section III. It determines the maximum number of CZ gates that the mapping and scheduling approach can tolerate with frequency crowding. In the following mapping and scheduling approach, we will explain how to leverage these local windows to achieve crosstalk and decoherence suppression across the entire chip.

C. Mapping algorithm

1) *Key design*: Our primary design strategy involves a delay in gate execution when the parallel constraint Eq. (3) is violated. This delay results in an extension of the execution time, denoted as t_{end} . We define a score function to evaluate the quality of the mapping, as shown in Eq. (4):

$$\text{score} = \frac{|g_{\text{exc}}| - 3|s|}{t_{\text{end}}}. \quad (4)$$

Here, the numerator serves as a reward, where $|g_{\text{exc}}|$ denotes the number of gates that can be executed, and $|s|$ represents the number of swap gates inserted, encouraging more gate executions and fewer swap gates. The denominator, representing the execution time t_{end} , serves as a penalty, discouraging mappings susceptible to significant crosstalk and longer execution times.

Consequently, CAMEL effectively aims to minimize both decoherence and crosstalk. As illustrated in Fig. 6(a), three CZ gates are ready for execution. Fig. 6(b) and (c) illustrate two distinct mappings. Given the maximum window size of 2×2 , the mapping in (b) satisfies the constraint, while the mapping in (c) does not. Consequently, at least one gate in (c) is delayed due to crosstalk, whereas all three gates in (b) can be executed in parallel. Our algorithm encourages the mapping of (b) over (c).

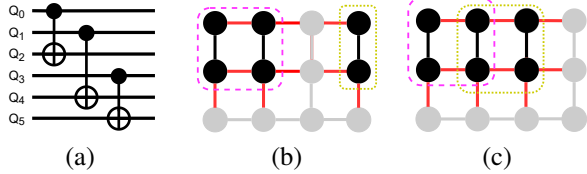


Fig. 6: (a) The circuit comprises three CZ gates. (b) and (c) depict two distinct mappings on the chip. In (b), the mapping of CZ gates to two disjoint windows satisfies the constraint, while the mapping in (c) violates the constraint.

The algorithm outlined in Alg. 1 details the crosstalk-aware mapping process. It starts by initializing a random mapping π_0 and an empty DAG \mathcal{D}_o . Then, it iterates over the gate set g in \mathcal{D} , utilizing the function **searchForward** to identify a subset of gates g_{exc} for minimal noise execution. This function receives the current mapping π_l , DAG \mathcal{D} , as well as the search depth L and search width W as its inputs. Gates from g_{exc} are then transferred from \mathcal{D} to \mathcal{D}_o . Finally, any swap gates in g_{exc} are applied to update the current mapping π_l .

2) *Recursive searching forward*: The Alg. 2 defines the **searchForward** function, which identifies a subset of gates for execution with minimal crosstalk, based on the current mapping π_l , input DAG \mathcal{D} , search depth L , and search width W . It begins by retrieving the top layer F of gates from the input DAG. An empty list g_{exc} is initialized to store executable gates, which are selected based on coupler connection constraint and the current mapping π_l . After adding suitable gates to g_{exc} , they are removed from the input DAG \mathcal{D} . If the search depth L is zero, the function returns g_{exc} . For each swap gate s in \mathcal{S} , the function calculates a distance sum d for the gates in F under the new mapping π_{l+1} . Afterward, the function proceeds by iterating through the first W swap

Algorithm 1 Crosstalk-aware mapping

Require: Coupling Graph $\mathcal{G}(\mathcal{Q}, \mathcal{E})$, DAG $\mathcal{D}(\mathbf{g}, \mathbf{g}, \mathbf{e})$, search depth L , search width W

Ensure: new DAG \mathcal{D}_o after compilation

- 1: get the remaining gate set \mathbf{g} in \mathcal{D}
 - 2: get a random initial mapping π_0
 - 3: let \mathcal{D}_o be a empty DAG
 - 4: **while** $\mathbf{g} \neq \emptyset$ **do**
 - 5: current mapping is π_l ,
 - 6: $g_{\text{exc}} = \text{searchForward}(\pi_l, \mathcal{D}, L, W)$
 - 7: remove the gates g_{exc} in \mathcal{D}
 - 8: apply the gates g_{exc} to \mathcal{D}_o
 - 9: **for** g in g_{exc} **do**
 - 10: **if** g is swap gate **then**
 - 11: apply g to π_l and get π_{l+1}
 - 12: $\pi_l \leftarrow \pi_{l+1}$
 - 13: **end if**
 - 14: **end for**
 - 15: get the remaining gate set \mathbf{g} in \mathcal{D}
 - 16: **end while**
-

gates s in the set \mathcal{S} , prioritized in ascending order of d . Each swap gate s is applied to the current mapping π_l , generating a new mapping π_{l+1} . It then proceeds to recursively call itself with the updated parameters, including the new mapping π_{l+1} , new DAG \mathcal{D} , decreased search depth $L - 1$, and the same search width W . This recursive call yields a list of executable gates $g_{\text{exc}2}$. The function evaluates the quality of the mapping π_{l+1} by calculating its score using the **scoreStep** function Alg. 3. If the score of the mapping π_{l+1} surpasses the current maximum score (**maxMapScore**), it updates **maxMapScore** and records the list of gates $g_{\text{exc},\text{best}}$ as the best choice for the current iteration. After iterating over the first W swap gates, the function returns the list of executable gates $g_{\text{exc}} + g_{\text{exc},\text{best}}$.

3) *Scoring strategy*: The purpose of function **scoreStep** in Alg. 3 is to evaluate the score of a current mapping and a list of executable gates. It initializes a dictionary Q_t to track the time of each physical qubit, and creates a list layers to accommodate gates that can execute parallelly. Additionally, it sets $|s|$ to store the count of swap gates in the list of executable gates g_{exc} . The algorithm then iterates over the gates g in g_{exc} , applying swap gates in g_{exc} to update the map. For each gate g , the algorithm assesses whether it overlaps with gates in the current layer. If it satisfies Eq. (2) and Eq. (3) alongside the gates in the layer, g is placed in the layer; otherwise, it is delayed. Additionally, if g does not overlap with existing gates, a new layer is created. After processing all gates, the algorithm calculates the mapping score Eq. (4) based on the number of executable gates, swap gates, and execution time.

4) *Complexity analysis*: The complexity of Alg. 3 depends on the number of iterations in the gate set $|g|$ and the number of layers L , resulting in a time complexity of $O(|g|L)$. The most resource-intensive operation occurs in the recursive call of Alg. 2. Here, the algorithm makes a maximum of W recursive calls, each with reduced depth $L - 1$. Thus, the time

Algorithm 2 Function searchForward

Require: π_l, \mathcal{D}, L, W **Ensure:** executable gates g_{exc}

```
1: get the top layer  $F$ 
2:  $g_{exc} = []$ 
3: add the  $g$  in  $F$  satisfied coupler connection constraint to
    $g_{exc}$ 
4: remove  $g_{exc}$  from  $\mathcal{D}$ 
5: if  $L = 0$  then
6:   return  $g_{exc}$ 
7: end if
8: for  $s$  in  $\mathcal{S}$  do
9:   apply  $s$  to  $\pi_l$  and get  $\pi_{l+1}$ 
10:   $d \leftarrow \sum_{g \in F} D(\pi_{l+1}(g.q_1), \pi_{l+1}(g.q_2))$ 
11: end for
12:  $\text{maxMapScore} = -\infty$ 
13: for the first  $W$   $s$  in  $\mathcal{S}$  in ascending order  $d$  do
14:   apply  $s$  to  $\pi_l$  and get  $\pi_{l+1}$ 
15:    $g_{exc2} = \text{searchForward}(\pi_{l+1}, \mathcal{D}, L - 1, W)$ 
16:    $\text{mapScore} \leftarrow \text{scoreStep}(\pi_l, g_{exc} + s + g_{exc2})$ 
17:   if  $\text{mapScore} > \text{maxMapScore}$  then
18:      $g_{exc, \text{best}} \leftarrow s + g_{exc2}$ 
19:   end if
20: end for
21: return  $g_{exc} \leftarrow g_{exc} + g_{exc, \text{best}}$ 
```

complexity is described by the recurrence relation:

$$\begin{aligned} T(L, W) &= WT(L - 1, W) + O(W|g|L), \\ &= W^L T(0, W) + O\left(\sum_{l=0}^{L-1} W^l |g|L\right), \quad (5) \\ &= O(W^L(|g|L + 1)). \end{aligned}$$

Here, $|g|$ represents the number of gates in \mathcal{D} . Since Alg. 1 calls the **searchForward** function at most $|g|$ times, once for each gate in the original DAG, the time complexity can be expressed as $O(|g|W^L(|g|L + 1)) = O(W^L|g|^2L)$. Notably, this complexity is polynomial with respect to the circuit scale $|g|$.

D. Gate scheduling algorithm

As the mapping algorithm is heuristic, it cannot entirely eliminate the gate time delay problem resulting from frequency crowding. Consequently, finding an optimal way to select a gate execution order that minimizes the circuit execution time becomes necessary.

1) *Barrier inserting:* The Alg. 4 takes the DAG $\mathcal{D}(q, g, e)$ and the coupling graph $\mathcal{G}(Q, E)$ as inputs. It produces the gate time for each gate in the circuit. Initially, the algorithm utilizes the function **extractGateTime** to assign gate times based on gate durations and circuit dependencies. Subsequently, it arranges the gates into layers, where gates within each layer overlap in time. Next, the algorithm employs the function **generatePartition** to divide the layers into sub-layers, ensuring that gates within each sub-layer can be executed parallelly without violating Eq. (3). To ensure sequential execution of

Algorithm 3 Function scoreStep

Require: π, g_{exc} **Ensure:** score

```
1:  $Q_t \leftarrow$  a dictionary with  $Q_t[Q] = 0, \forall Q \in \mathcal{Q}$ 
2: layers  $\leftarrow []$ 
3:  $|s| \leftarrow$  the number of gate  $g \in \mathcal{S}$ 
4: for  $g$  in  $g_{exc}$  do
5:   if  $g \in \mathcal{S}$  then
6:     apply  $g$  to  $\pi$  and get a new  $\pi$ 
7:   end if
8:   for layer in layers do
9:     if time interval  $(Q_t[\pi(g.q)], Q_t[\pi(g.q)] + t_g)$  has
       overlap with the gates in layer then
10:       $\mathcal{Q}_g \leftarrow \{\pi(g_l.q) | \forall g_l \in \text{layer} \cup g\}$  and induce  $\mathcal{G}_g$ 
        from  $\mathcal{Q}_g$  and  $\mathcal{G}$ 
11:      if there is not connected subgraph of  $\mathcal{G}_g$  violate
        the parallel constraint then
12:         $Q_t[\pi(g.q)] \leftarrow Q_t[\pi(g.q)] + t_g$ 
13:        layer.append( $g$ )
14:      else
15:         $t \leftarrow$  the maximum  $Q_t[\pi(g_l.q)]$  for gate qubits
         $g_l.q$  in layer
16:         $Q_t[\pi(g.q)] \leftarrow t$ 
17:      end if
18:    end if
19:  end for
20:  if there is no layer for  $g$  then
21:    layers.append( $[g]$ )
22:     $t \leftarrow$  the maximum time in  $Q_t$ 
23:     $Q_t[\pi(g.q)] \leftarrow t + t_g$ 
24:  end if
25: end for
26:  $t_{\text{end}} \leftarrow$  the maximum time in  $Q_t$ 
27: score =  $\frac{|g_{exc}| - 3|s|}{t_{\text{end}}}$ 
28: return score
```

gates across different sub-layers, barriers are inserted between gates among each layer. In the provided example shown in Fig. 7, due to the presence of barriers, the execution of the second CZ gate involving qubits q_2 and q_4 is delayed, as it relies on the barrier involving qubits $q_1, q_2,$ and q_3 .

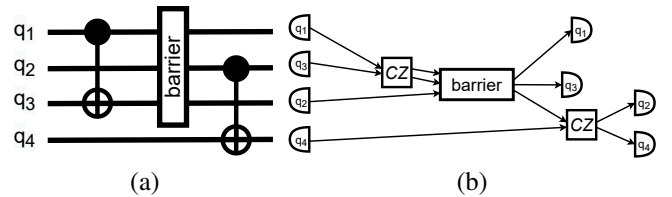


Fig. 7: (a) A barrier was inserted between these CZ gates. (b) Gate order is changed as follows: $\text{CZ}_1 < \text{barrier} < \text{CZ}_2$.

2) *Maximum-independent set partition:* To depict the crosstalk relationship between parallel gates, we first introduce the crosstalk graph $\mathcal{T}(g, X)$, where nodes g represent CZ gates executed parallelly in the same layer. An edge $x \in X$

Algorithm 4 Gate scheduling algorithm

Require: DAG $\mathcal{D}(q, g, e)$, Coupling Graph $\mathcal{G}(Q, E)$ **Ensure:** gTime

```
1: gTime=extractGateTime( $\mathcal{D}$ )
2: layers $\leftarrow$  []
3: for  $g$  in  $g$  do
4:   for layer in layers do
5:     if  $\exists g_l \in$  layer has execution time overlap with
       gTime[ $g$ ] then
6:       layer.append( $g$ )
7:     end if
8:   end for
9:   if there is no layer for  $g$  then
10:    layers.append([ $g$ ])
11:  end if
12: end for
13: partitions=generatePartition(layers, $\mathcal{G}$ )
14: for (partition, layer) in (partitions, layers) do
15:   add barrier to gates in layer according to partition
16: end for
17: gTime=extractGateTime( $\mathcal{D}$ )
18: return gTime
```

connects nodes if crosstalk exists between them, defined as:

$$\min(D(\pi(g_1.q), \pi(g_2.q))) = 1, \quad (6)$$
$$\Rightarrow (g_1, g_2) \in \mathbf{X}.$$

Eq. (6) implies that when the logical qubits of parallel CZ gates are mapped to physical qubits on the chip with a minimum distance of 1, crosstalk between the gates occurs.

In Alg. 5, the function **generatePartition** iterates over each layer to seek out the maximum-independent sets i.e., subsets of crosstalk-free gates within \mathcal{T} . Firstly, mapping the CZ gates in this layer to the chip. Initialize a window list l_{w_i} for each window w_i containing pending CZ gate in layer. Iterate through each window w_j on the chip, if w_j contains qubits with a minimum distance greater than 2 from all qubits in l_{w_i} , then w_j is added to l_{w_i} . This step aims to identify the largest set of non-adjacent windows that can be executed parallelly without crosstalk. Next, select the l_w with the max coverage of pending gates, forming a covering set capable of executing the max number of CZ gates simultaneously.

Following this, the coupler edges between CZ gates covered by windows are removed from the algorithm subgraph \mathcal{G}_g . This step indicates the mitigation of crosstalk between CZ gates covered by windows through compensation pulses. Based on the resulting \mathcal{G}_g after edge deletion, we obtain \mathcal{T} according to Eq. (6). Utilizing Python library Networkx [40], we apply the **maxIndependentSet** function to find solutions to maximum-independent set problem of \mathcal{T} in polynomial time.

Fig. 8 serves as an example. It's found that the window w_1 corresponding to q_0, q_4 and q_1, q_5 and another non-adjacent window w_2 corresponding to q_3, q_7 , cover the maximum of CZ gates. Consequently, the edges between the two gates within w_1 are removed, resulting in the crosstalk graph \mathcal{T} . Employing the **maxIndependentSet** function, \mathcal{T} is divided into two independent subgraphs. This indicates that the four

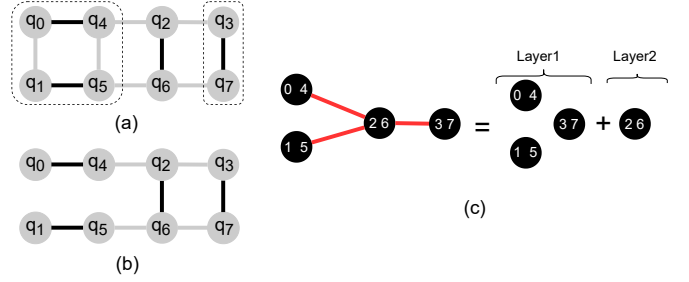


Fig. 8: (a) The mapping of CZ gates on chip, with black edges indicating activated couplers. Qubits q_0, q_4 and q_1, q_5 are covered by window w_1 , and q_3, q_7 are covered by another non-adjacent window w_2 . (b) The edges within these windows are deleted. (c) The crosstalk graph consists of nodes representing parallel gates from (a). This graph is partitioned into two maximum-independent sets.

Algorithm 5 Function generatePartition

Require: layers, Coupling Graph $\mathcal{G}(Q, E)$ **Ensure:** partitions is a dictionary which partitions[g] = i which means that g in the i^{th} partition

```
1: for layer in layers do
2:    $l = []$ 
3:   for window  $w_i$  include  $g \in$  layer on the chip do
4:      $l_{w_i} \leftarrow [w_i]$ 
5:     for window  $w_j \notin l_{w_i}$  on the chip do
6:       if all qubits in  $w_j$  with a distance  $> 2$  to all qubits
         in  $l_{w_i}$ . then
7:          $l_{w_i}.append(w_j)$ 
8:       end if
9:     end for
10:     $l.append(l_{w_i})$ 
11:  end for
12:  Select window list  $l_w$  in  $l$  which covers maximum qubit
    set of layer
13:  Remove coupler edges of  $\mathcal{G}_g$  between CZ gates covered
    by  $l_w$ 
14:  Calculate  $\mathcal{T}$  based on  $\mathcal{G}_g$  using Eq. (6)
15:  independentSets  $\leftarrow$  maxIndependentSet( $\mathcal{T}$ )
16:  Divide layer according to independentSets
17: end for
```

CZ gates will be split into two steps: the first step executes the gates between $[q_0, q_4]; [q_1, q_5]; [q_3, q_7]$, while the second step executes the gate between $[q_2, q_6]$.

3) *Complexity analysis:* The complexity of Alg. 5 is $O(|\mathcal{G}|(|\mathcal{G}| + N^2))$. Here, $|\mathcal{G}|$ represents the complexity of finding a maximum-independent set, and N denotes the number of qubits on the chip. N^2 indicates the complexity of identifying the maximum cover of pending gates. The **maxIndependentSet** function in Networkx has a complexity of $O(|\mathcal{G}|) = O(|\mathcal{G}|/(\log^2 |\mathcal{G}|))$ [40], where $|\mathcal{G}|$ corresponds to the node number of \mathcal{G} , which is at most the number of gates. Alg. 5 calls the **maxIndependentSet** function at most $|\mathcal{G}|$ times. Considering that Alg. 4 invokes Alg. 5 once and the complexities of the loop and **extractGateTime** are $|\mathcal{G}|^2$,

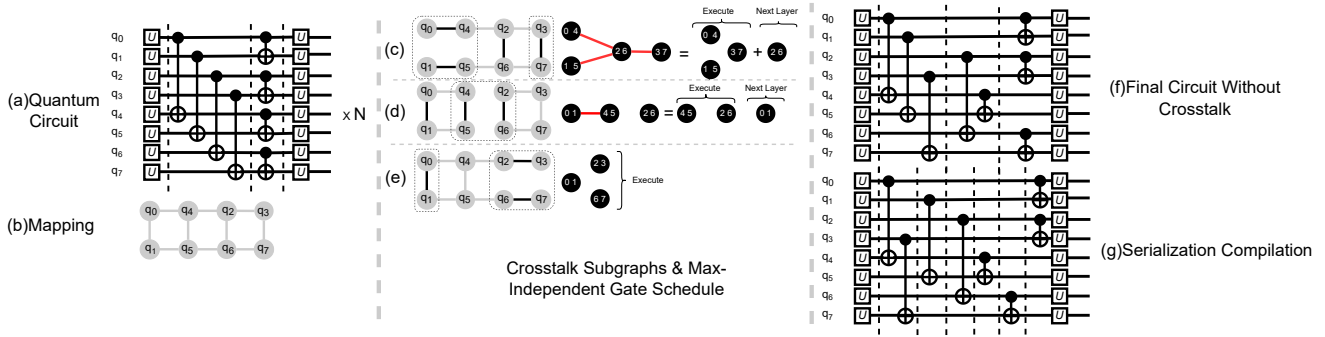


Fig. 9: The schematic of the compilation process is illustrated assuming our chip has a maximum calibration window size of 2×2 . (a) depicts a segment of the quantum circuit from the VQE algorithm [41]. In (b), a mapping to qubits on a 2×4 quantum chip is illustrated. (c-e) demonstrate the parallel execution on the chip of the top layer gates of the quantum circuit according to this mapping, accompanied by the corresponding crosstalk subgraph. In (c), it’s evident that executing $g_{q_0,q_4}, g_{q_1,q_5}, g_{q_2,q_6}, g_{q_3,q_7}$ parallelly violates the parallel constraint. On the other hand, our gate scheduling approach finds the maximum parallel execution of the first three gates: g_{q_0,q_4}, g_{q_1,q_5} , and g_{q_3,q_7} . (c-e) illustrate gate scheduling steps based on the maximum independent set. (f) presents the compiled circuit, completing execution in only three layers. Conversely, executing all crosstalk gates serially, as depicted in figure (g), would necessitate six layers, increasing decoherence.

the overall complexity amounts to $O(|g|^2 + |g|(|G| + N^2)) = O(|g|^2(1/(\log^2 |g|) + 1) + |g|N^2) = O(|g|^2 + |g|N^2)$.

V. EVALUATION

A. Baselines

In this section, we evaluate the CAMEL algorithm and compare it with several baselines as follows:

- **Crosstalk-agnostic compilation (N)**: This approach relies on fixed idle and interaction frequencies without optimization for crosstalk mitigation [42]–[45]. It employs a crosstalk-agnostic qubit mapper and a tiling gate scheduler. We adopt the Sabre approach as a representation of crosstalk-agnostic compilation [45].
- **Serialization compilation (S)**: This approach utilizes fixed idle and interaction frequencies without optimization for crosstalk mitigation [10], [11]. It employs a crosstalk-aware gate scheduler that serializes parallel CZ gates. We adopt the approach proposed by Murali et al. [10] to represent serialization compilation.
- **Static frequency-aware compilation (SF)**: In this approach, idle and interaction frequencies are fixed and optimized for crosstalk mitigation [22]. It employs a crosstalk-aware gate scheduler. We utilize the snake optimizer as a representation of static frequency-aware compilation.
- **Dynamic frequency-aware compilation (DF)**: Idle frequencies remain fixed while interaction frequencies are dynamically optimized for each quantum circuit. Additionally, this approach utilizes a crosstalk-aware gate scheduler. We adopt Ding’s approach [20] as a baseline of this type.
- **CAMEL (this paper)**: CAMEL utilizes a crosstalk-aware mapper and gate scheduler, which employs fixed optimized idle and interaction frequencies, along with compensation pulse to mitigate crosstalk.

B. Architectural features

We consider a chip architecture consisting of a 2D grid of $N \times N$ frequency-tunable qubits and couplers. The qubits operate within a frequency range of $\omega_q \in (4, 5)$ GHz, while the couplers span $\omega_c \in (5, 7)$ GHz. The anharmonicity values for the couplers and qubits are approximately $\eta_c \approx -100$ MHz and $\eta_q \approx -200$ MHz, respectively. The coupling strengths are $g_{ic} \approx 100$ MHz and $g_{12} \approx 10$ MHz. Each frequency-tunable qubit is connected via frequency-tunable couplers. The decoherence times T_i are modeled based on [4]. Additionally, both initial and measurement errors are set within a range of 0.01 ± 0.001 . These values are obtained from experimental data reported in the literature [46].

C. Benchmarks

We evaluate the performance of our algorithm using NISQ benchmarks from [41], which represent key applications for near-term quantum devices. In addition, we use cross entropy benchmarking (XEB) circuits [23] to demonstrate the effect of crosstalk on gate fidelity.

- **Simple quantum algorithms**: Including Simon’s algorithm and the Quantum Fourier Transform (QFT).
- **Quantum optimization algorithm**: Quantum Approximate Optimization Algorithm (QAOA) [47] applied to MAX-CUT on an Erdős-Rényi random graph.
- **Variational quantum algorithm**: Using the Variational Quantum Eigensolver (VQE) to determine the ground state energy of molecules.
- **Quantum machine learning algorithm**: Utilizing Quantum Generative Adversarial Networks (QGAN).
- **Cross entropy benchmarking**: Using XEB circuits with 16 qubits and 200 cycles.

D. Software implementation

Quantum gates and circuits are simulated using Qutip [48]. The graph algorithm is implemented using Networkx [40].

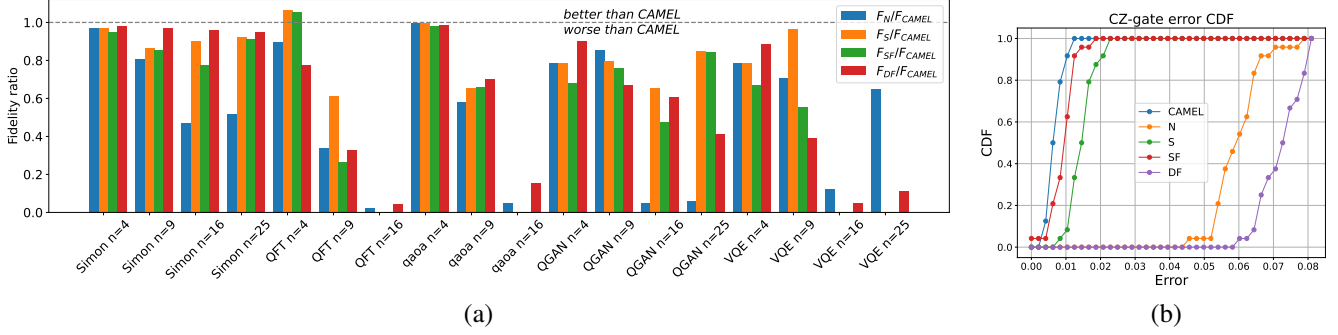


Fig. 10: (a) The fidelity of the Simon algorithm, QFT algorithm, QAOA algorithm, QGAN algorithm, and VQE algorithm after being compiled with different baselines. We have computed the fidelity ratios between all baselines and CAMEL approach. The gray dashed line represents a ratio of one. Bars above the dashed line indicate better performance than CAMEL, while bars below the dashed line indicate worse performance. Some results for 16 and 25-qubit QFT, QAOA, and VQE algorithms are absent due to the excessive simulation time. It can be observed that CAMEL approach consistently maintains high fidelity. (b) The XEB experiment of the approaches. Through parallel XEB circuits, the error of each two-qubit gate on the chip can be obtained, resulting in a cumulative distribution function (CDF) plot. CAMEL have the lowest error distribution, the second is static-frequency aware compilation, and then, serialization compilation, crosstalk-agnostic compilation and the worst one is dynamic-frequency-aware compilation.

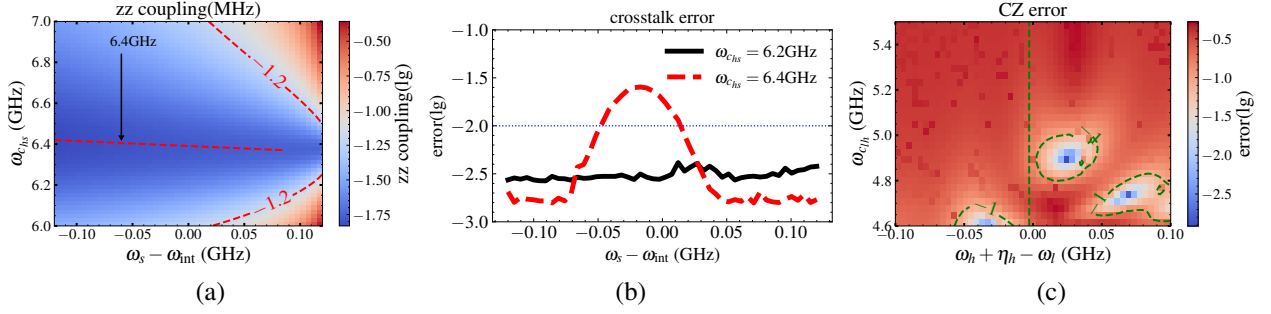


Fig. 11: (a) The graph illustrates the minimum ZZ-coupling occurring around $\omega_{chs} = 6.4$ GHz, with spectator qubit frequency situated around ω_{int} . (b) During CZ gate execution, if we don't adjust the coupler frequency to 6.2 GHz when ω_s and ω_{int} collide, the error will increase to 10^{-2} . (c) Let $\omega_l = \omega_h + \eta_h = \omega_{int}$ be the interaction frequency. The actual interaction frequency deviates from the initially set interaction frequency. Under the initial interaction frequency, the error does not drop below 10^{-1} .

Simulating a quantum circuit Hamiltonian at the pulse level is highly unscalable. To incorporate crosstalk effects into the simulation, we examine Eq. (1), which represents the population swap from gate state $|020\rangle$ to population swap state $|110\rangle$. The coupling strength g_{xtalk} can be determined from the qubit frequency configuration. Apply a coordinate transformation $U = \exp(\frac{i}{\hbar}H_0)$, and we obtain:

$$H = UHU^\dagger - i\hbar\dot{U}U^\dagger = \begin{pmatrix} 0 & g_{xtalk} \exp(\frac{i\Delta_{gs}t}{\hbar}) \\ g_{xtalk} \exp(\frac{\Delta_{gs}t}{i\hbar}) & 0 \end{pmatrix}, \quad (7)$$

where $\Delta_{gs} = E_{020} - E_{110}$. When the frequency crowding occurs, $\Delta_{gs} \approx 0$. Thus Eq. (7) can be rewritten as:

$$H/\hbar = \begin{pmatrix} 0 & g_{xtalk} \\ g_{xtalk} & 0 \end{pmatrix}. \quad (8)$$

Eq. (8) can be solved as a unitary transformation between the states $|110\rangle$ and $|020\rangle$.

$$\begin{pmatrix} \cos g_{xtalk}t_g & -i \sin g_{xtalk}t_g \\ -i \sin g_{xtalk}t_g & \cos g_{xtalk}t_g \end{pmatrix}, \quad (9)$$

which means that during the gate execution time t_g , the population swap from the gate state $|020\rangle$ to the population swap state $|110\rangle$ can be modeled as a unitary transformation, i.e., a quantum gate. Firstly, we calculate $|E_{020} - E_{110}|$ based on the frequency configuration to identify whether $|020\rangle$ experiences population swap. Secondly, we determine g_{xtalk} according to frequency configuration. After executing the two-qubit gate on Q_1 and Q_2 , we apply the quantum gate Eq. (9) to Q_1 , Q_2 , and Q_s . The simulation is still performed at the gate level, avoiding the direct Hamiltonian simulation of pulses.

E. Results

Fig. 10(a) is the comparison of compiled circuits fidelity. Each bar is the fidelity ratio between compared baseline and

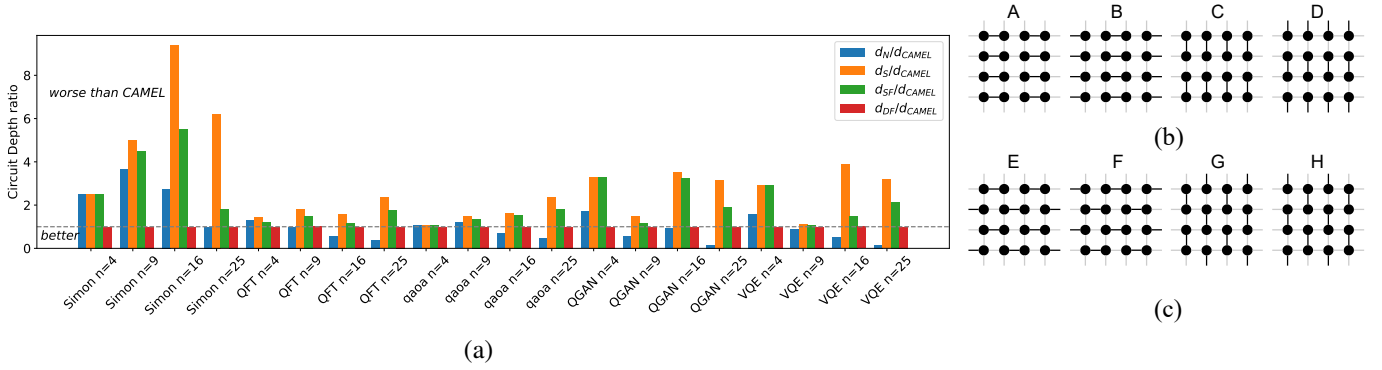


Fig. 12: (a) The depth ratio of benchmark circuits compiled with different baselines. The gray dashed line represents a ratio of one. As depicted, the time durations corresponding to the serialization and static frequency baselines are generally longer than those of CAMEL. (b-c) Coupler activation patterns. Coupler activation pattern determines which qubits are allowed to execute CZ gate simultaneously in a cycle. ABCD patterns in (b) are exclusive from the EFGH in (c).

CAMEL approach, the higher the better. The gray dashed line represented ratio one. Based on Fig. 10(a), the fidelity of CAMEL is generally higher than that of other approaches. In the XEB experiment Fig. 10(b), CAMEL has the lowest CZ gate error distribution. Next, we will proceed to compare and explain each case individually.

1) *Comparison with crosstalk-agnostic compilation:* Our algorithm consistently achieves higher fidelity compared to the crosstalk-agnostic compilation baseline due to its consideration of crosstalk. The crosstalk-agnostic approach overlooks crosstalk, resulting in frequency collisions and significantly lower gate fidelity. In Fig. 11(a-b), we analyze a three-qubit model denoted as $|Q_s Q_h Q_l\rangle$. Here, Q_s represents the spectator qubit, while Q_h and Q_l correspond to the high-frequency and low-frequency qubits involved in gates, respectively. When the CZ gate involving Q_h and Q_l is not executed, the ZZ-coupling reaches its minimum value around 6.4 GHz. During the execution of the CZ gate, we have $\omega_l = \omega_h + \eta_h = \omega_{\text{int}}$. If $\omega_{c_{h,s}} = 6.4$ GHz, there will be a frequency range of about 100 MHz for ω_s where the CZ error is larger than 10^{-2} . Q_l and Q_s are both coupled with Q_h . Considering the frequency crowding problem, ω_s is allocated around ω_{int} and likely to fall within the error large range. CAMEL uses compensation pulses to tune the $c_{h,s}$ frequency from 6.4 GHz to 6.1 GHz, ensuring low error.

2) *Comparison with dynamic frequency-aware compilation:* CAMEL is better than the dynamic frequency-aware compilation baseline in terms of fidelity. Dynamic frequency-aware compilation requires dynamically allocating the interaction frequency for CZ gates activated by the algorithm subgraph. Otherwise, real-time frequency configuration, without gate parameter calibration, tends to result in low fidelity of CZ gates. From Fig. 11(c), when the low-frequency qubit is adjusted to $\omega_{l,\text{on}}$, the corresponding high-frequency qubit should be adjusted to $\omega_{l,\text{on}} - \eta_h$. However, at this frequency, there is no coupler frequency that can achieve an error lower than 10^{-1} . Actually, there is a deviation between the set interaction frequency and the actual interaction frequency, necessitating calibration. Implementing dynamic frequency configuration would require calibration before each activated

algorithm subgraph, which would require an infeasible task of multiple iterations of gate parameter optimization during circuit execution.

3) *Comparison with serialization and static frequency-aware compilation:* CAMEL consistently outperforms the serialization compilation baseline in terms of fidelity. This can be understood by looking at Fig. 12(a), which displays the depth ratio of compiled circuits. The orange bars are higher than the gray dashed line, indicating that the compiled circuits take longer time to execute than CAMEL. This occurs because the serialization baseline serializes all crosstalk gates, thereby increasing the execution time. Consequently, this amplifies the impact of decoherence.

Now we explain why static frequency-aware compilation baselines (green bars) have longer execution time. Not all two-qubit gates can be executed simultaneously, and Fig. 12(b-c) illustrates the eight maximum parallel patterns for the CZ gate. If a static frequency-aware compilation method is applied, with frequency configuration and calibration based on the first (last) four patterns, multiple CZ gates within any one of the ABCD (EFGH) patterns can be executed in parallel. While a quantum circuit may necessitate various scenarios of parallelism, especially, parallel execution between CZ gates in distinct patterns, fixed-frequency configuration fails to accommodate such requirements. Thus, the serialization method is still required in the presence of crosstalk, leading to an increase in execution time.

4) *Ablation study:* This section evaluates the effects of compensation pulses and the crosstalk-aware mapper and gate scheduler separately.

With and without compensation pulse: Experiments with window sizes from 0 to 4×4 are done in this step. The baselines are serialization compilation the static frequency-aware compilation approaches. We use 200-layer, 4×4 XEB circuits as benchmarks.

When the window size is set to 0, CAMEL is equivalent to serialization compilation. As shown in Fig. 13(a), CAMEL performs similarly to serialization compilation with a window size of 0. However, as the window size increases, CAMEL demonstrates improved performance. Specifically, the XEB

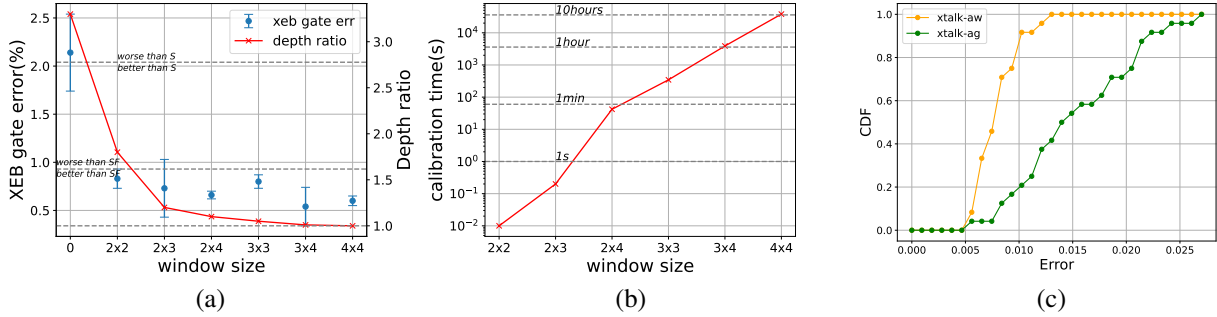


Fig. 13: (a) The XEB error decreases as the window size increases from 0 to 4×4 . Starting at 2×2 , the error approaches the level of static frequency-aware compilation and continues to drop. Additionally, the ratio of the circuit execution time after and before compilation decreases as the window size increases. (b) The calibration time grows exponentially as window size increases. (c) The cumulative distribution function (CDF) plot of errors from the XEB experiment. The green curve represents the results compiled using the crosstalk-agnostic approach, while the yellow curve shows the results compiled using the crosstalk-aware mapper and scheduler.

error decreases and the execution time ratio approaches 1, although the gains become marginal. Fig. 13(b) illustrates that the calibration time grows exponentially with the window size. At a window size of 2×2 , the XEB error is already lower than that of static frequency-aware compilation. This supports the choice of a 2×2 window as an optimal balance between fidelity and calibration time.

Within the calibrated window, all parallel two-qubit gate situations are considered, and all frequency crowding scenarios can be mitigated by compensation pulses. This window size introduces maximum allowable parallelism in the subsequent mapping and scheduling steps, increasing the solution space for the mapping and scheduling approach, making it easier to find an optimal solution.

With and without mapping and scheduling: In this step, we conduct a control experiment comparing the crosstalk-agnostic approach with the crosstalk-aware mapper and scheduler (the full CAMEL) on a chip after frequency configuration and pulse calibration. We performed frequency configuration based on the ABCD coupler activation pattern and calibrated the compensation pulse for each 2×2 window. An XEB experiment with four randomly selected maximum parallel coupler activation patterns were conducted.

As shown in Fig. 13(c), the error distribution of CAMEL is lower than that of the crosstalk-agnostic approach. This is because the crosstalk-agnostic approach fails to account for frequency crowding and, when encountering cases where compensation pulses cannot fully address the crowding, it does not optimize the mapping or scheduling. Without mapping and scheduling, for the window size is much smaller than the chip size, frequency crowding can only be mitigated locally. In contrast, CAMEL’s mapper and scheduler are capable of detecting and mitigating frequency crowding in arbitrary quantum circuits. The CAMEL mapping and scheduling components use a heuristic approach to extend the local crosstalk mitigation capability of the compensation pulse to the entire chip.

VI. CONCLUSION

In summary, we propose a compilation approach to mitigate crosstalk and decoherence in superconducting frequency-tunable quantum chips. Our method first numerically validates that applying compensation pulses to the spectator coupler effectively reduces crosstalk, particularly in scenarios where frequency crowding occurs. To tackle the challenge of optimizing compensation pulses for arbitrary parallel patterns, we introduced a sliding window approach. Building on this, we developed a crosstalk-aware qubit mapping strategy and a gate timing scheduling method named “CAMEL”. Through numerical experiments and comparisons with existing frequency configuration compilation methods, CAMEL shows notable improvements in reducing crosstalk and achieving shorter execution times for common NISQ benchmark circuits on lattice-structured superconducting quantum chips. CAMEL presents a promising step toward developing robust and scalable quantum computing systems, providing a foundation for future large-scale quantum error correction circuits that require the parallel execution of multiple CZ gates.

ACKNOWLEDGEMENTS

This work has been supported by the National Key Research and Development Program of China (Grant No. 2023YFB4502500).

REFERENCES

- [1] John Preskill. Quantum computing in the nirq era and beyond. *Quantum*, 2:79, 2018.
- [2] Philip Krantz, Morten Kjaergaard, Fei Yan, Terry P Orlando, Simon Gustavsson, and William D Oliver. A quantum engineer’s guide to superconducting qubits. *Applied physics reviews*, 6(2), 2019.
- [3] Jonas Bylander, Simon Gustavsson, Fei Yan, Fumiki Yoshihara, Khalil Harrabi, George Fitch, David G Cory, Yasunobu Nakamura, Jaw-Shen Tsai, and William D Oliver. Noise spectroscopy through dynamical decoupling with a superconducting flux qubit. *Nature Physics*, 7(7):565–570, 2011.
- [4] G Ithier, E Collin, P Joyez, PJ Meeson, Denis Vion, Daniel Esteve, F Chiarello, A Shnirman, Yu Makhlin, Josef Schrieffer, et al. Decoherence in a superconducting quantum bit circuit. *Physical Review B*, 72(13):134519, 2005.

- [5] Fei Yan, Simon Gustavsson, Archana Kamal, Jeffrey Birenbaum, Adam P Sears, David Hover, Ted J Gudmundsen, Danna Rosenberg, Gabriel Samach, Steven Weber, et al. The flux qubit revisited to enhance coherence and reproducibility. *Nature communications*, 7(1):12964, 2016.
- [6] Sebastian Krinner, Stefania Lazar, Ants Remm, Christian K Andersen, Nathan Lacroix, Graham J Norris, Christoph Hellings, Mihai Gabureac, Christopher Eichler, and Andreas Wallraff. Benchmarking coherent errors in controlled-phase gates due to spectator qubits. *Physical Review Applied*, 14(2):024042, 2020.
- [7] Carmen G Almudever, Lingling Lao, Xiang Fu, Nader Khammassi, Imran Ashraf, Dan Iorga, Savvas Varsamopoulos, Christopher Eichler, Andreas Wallraff, Lotte Geck, et al. The engineering challenges in quantum computing. In *Design, Automation & Test in Europe Conference & Exhibition (DATE)*, 2017, pages 836–845. IEEE, 2017.
- [8] Marcos Yukio Siraichi, Vinícius Fernandes dos Santos, Caroline Collange, and Fernando Magno Quintão Pereira. Qubit allocation as a combination of subgraph isomorphism and token swapping. *Proceedings of the ACM on Programming Languages*, 3(OOPSLA):1–29, 2019.
- [9] Marcos Yukio Siraichi, Vinícius Fernandes dos Santos, Caroline Collange, and Fernando Magno Quintão Pereira. Qubit allocation. In *Proceedings of the 2018 International Symposium on Code Generation and Optimization*, pages 113–125, 2018.
- [10] Prakash Murali, David C McKay, Margaret Martonosi, and Ali Javadi-Abhari. Software mitigation of crosstalk on noisy intermediate-scale quantum computers. In *Proceedings of the Twenty-Fifth International Conference on Architectural Support for Programming Languages and Operating Systems*, pages 1001–1016, 2020.
- [11] Fei Hua, Yuwei Jin, Yan-Hao Chen, Chi Zhang, Ari B. Hayes, Hang Gao, and Eddy Z. Zhang. Cqc: A crosstalk-aware quantum program compilation framework. 2022.
- [12] ADK Finck, S Carnevale, D Klaus, Chris Scerbo, J Blair, TG McConkey, Cihan Kurter, A Carniol, George Keefe, Muir Kumph, et al. Suppressed crosstalk between two-junction superconducting qubits with mode-selective exchange coupling. *Physical Review Applied*, 16(5):054041, 2021.
- [13] Jaseung Ku, Xuexin Xu, Markus Brink, David C McKay, Jared B Hertzberg, Mohammad H Ansari, and BLT Plourde. Suppression of unwanted z interactions in a hybrid two-qubit system. *Physical review letters*, 125(20):200504, 2020.
- [14] Zhongchu Ni, Sai Li, Libo Zhang, Ji Chu, Jingjing Niu, Tongxing Yan, Xiuhao Deng, Ling Hu, Jian Li, Youpeng Zhong, et al. Scalable method for eliminating residual z interaction between superconducting qubits. *Physical review letters*, 129(4):040502, 2022.
- [15] KX Wei, E Magesan, I Lauer, S Srinivasan, DF Bogorin, S Carnevale, GA Keefe, Y Kim, D Klaus, W Landers, et al. Quantum crosstalk cancellation for fast entangling gates and improved multi-qubit performance. *arXiv preprint arXiv:2106.00675*, 2021.
- [16] Peng Zhao, Dong Lan, Peng Xu, Guangming Xue, Mace Blank, Xinsheng Tan, Haifeng Yu, and Yang Yu. Suppression of static z interaction in an all-transmon quantum processor. *Physical Review Applied*, 16(2):024037, 2021.
- [17] Pranav Mundada, Gengyan Zhang, Thomas Hazard, and Andrew Houck. Suppression of qubit crosstalk in a tunable coupling superconducting circuit. *Physical Review Applied*, 12(5):054023, 2019.
- [18] Youngkyu Sung, Leon Ding, Jochen Braumüller, Antti Vepsäläinen, Bharath Kannan, Morten Kjaergaard, Ami Greene, Gabriel O Samach, Chris McNally, David Kim, et al. Realization of high-fidelity cz and z -free $iswap$ gates with a tunable coupler. *Physical Review X*, 11(2):021058, 2021.
- [19] Paul V Klimov, Andreas Bengtsson, Chris Quintana, Alexandre Bourassa, Sabrina Hong, Andrew Dunsworth, Kevin J Satzinger, William P Livingston, Volodymyr Sivak, Murphy Yuezhen Niu, et al. Optimizing quantum gates towards the scale of logical qubits. *Nature Communications*, 15(1):2442, 2024.
- [20] Yongshan Ding, Pranav Gokhale, Sophia Fuhui Lin, Rich Rines, Thomas P. Propson, and Frederic T. Chong. Systematic crosstalk mitigation for superconducting qubits via frequency-aware compilation. *2020 53rd Annual IEEE/ACM International Symposium on Microarchitecture (MICRO)*, pages 201–214, 2020.
- [21] Nicolas Wittler, Federico Roy, Kevin Pack, Max Werninghaus, Anurag Saha Roy, Daniel J Egger, Stefan Filipp, Frank K Wilhelm, and Shai Machnes. Integrated tool set for control, calibration, and characterization of quantum devices applied to superconducting qubits. *Physical review applied*, 15(3):034080, 2021.
- [22] Paul V Klimov, Julian Kelly, John M Martinis, and Hartmut Neven. The snake optimizer for learning quantum processor control parameters. *arXiv preprint arXiv:2006.04594*, 2020.
- [23] Frank Arute, Kunal Arya, Ryan Babbush, Dave Bacon, Joseph C Bardin, Rami Barends, Rupak Biswas, Sergio Boixo, Fernando GSL Brandao, David A Buell, et al. Quantum supremacy using a programmable superconducting processor. *Nature*, 574(7779):505–510, 2019.
- [24] Joseph Clark, Travis Humble, and Himanshu Thapliyal. Tdag: Tree-based directed acyclic graph partitioning for quantum circuits. In *Proceedings of the Great Lakes Symposium on VLSI 2023*, GLSVLSI '23, page 587–592, New York, NY, USA, 2023. Association for Computing Machinery.
- [25] Clemens Müller, Jürgen Lisenfeld, Alexander Shnirman, and Stefano Poletto. Interacting two-level defects as sources of fluctuating high-frequency noise in superconducting circuits. *Physical Review B*, 92(3):035442, 2015.
- [26] Sergey Bravyi, David P DiVincenzo, and Daniel Loss. Schrieffer–wolf transformation for quantum many-body systems. *Annals of physics*, 326(10):2793–2826, 2011.
- [27] Matteo Mariantoni, H. Wang, T. Yamamoto, M. Neeley, and John M Martinis. Implementing the quantum von neumann architecture with superconducting circuits. *Science*, 334(6052):61–65, 2011.
- [28] Sirui Cao, Bujiao Wu, Fusheng Chen, Ming Gong, Yulin Wu, Yangsen Ye, Chen Zha, Haoran Qian, Chong Ying, and Shaojun Guo. Generation of genuine entanglement up to 51 superconducting qubits. *Nature*, 2023.
- [29] Suppressing quantum errors by scaling a surface code logical qubit. *Nature*, 614(7949):676–681, 2023.
- [30] Rajeev Acharya, Laleh Aghababaei-Beni, Igor Aleiner, Trond I Andersen, Markus Ansmann, Frank Arute, Kunal Arya, Abraham Asfaw, Nikita Astrakhantsev, Juan Atalaya, et al. Quantum error correction below the surface code threshold. *arXiv preprint arXiv:2408.13687*, 2024.
- [31] Peng Zhao, Kehuan Linghu, Zhiyuan Li, Peng Xu, Ruixia Wang, Guangming Xue, Yirong Jin, and Haifeng Yu. Quantum crosstalk analysis for simultaneous gate operations on superconducting qubits. *PRX quantum*, 3(2):020301, 2022.
- [32] Peng Zhao, Yingshan Zhang, Xuegang Li, Jiaxiu Han, Huikai Xu, Guangming Xue, Yirong Jin, and Haifeng Yu. Spurious microwave crosstalk in floating superconducting circuits. *arXiv preprint arXiv:2206.03710*, 2022.
- [33] Lei Xie, Jidong Zhai, Zhenxing Zhang, Jonathan Allcock, Shengyu Zhang, and Yicong Zheng. Suppressing zz crosstalk of quantum computers through pulse and scheduling co-optimization. *Proceedings of the 27th ACM International Conference on Architectural Support for Programming Languages and Operating Systems*, 2022.
- [34] Paul Klimov, Julian Kelly, Kevin Satzinger, Zijun Chen, Hartmut Neven, and John Martinis. Optimizing quantum gate frequencies for google’s quantum processors. *Bulletin of the American Physical Society*, 65, 2020.
- [35] Ji Chu and Fei Yan. Coupler-assisted controlled-phase gate with enhanced adiabaticity. *Physical Review Applied*, 16(5):054020, 2021.
- [36] DM Zajac, J Stehlik, DL Underwood, T Phung, J Blair, S Carnevale, D Klaus, GA Keefe, A Carniol, M Kumph, et al. Spectator errors in tunable coupling architectures. *arXiv preprint arXiv:2108.11221*, 2021.
- [37] Wojciech Samotij. Counting independent sets in graphs. *European journal of combinatorics*, 48:5–18, 2015.
- [38] Min-Jen Jou and Gerard J Chang. The number of maximum independent sets in graphs. *Taiwanese Journal of Mathematics*, 4(4):685–695, 2000.
- [39] Omar Shindi, Qi Yu, Parth Girdhar, and Daoyi Dong. Model-free quantum gate design and calibration using deep reinforcement learning. *IEEE Transactions on Artificial Intelligence*, 2023.
- [40] Aric Hagberg and Drew Conway. Networkx: Network analysis with python. URL: <https://networkx.github.io>, 2020.
- [41] Adetokunbo Adedoyin, John Ambrosiano, Petr Anisimov, William Casper, Gopinath Chennupati, Carleton Coffrin, Hristo Djidjev, David Gunter, Satish Karra, Nathan Lemons, et al. Quantum algorithm implementations for beginners. *arXiv preprint arXiv:1804.03719*, 2018.
- [42] Chi Zhang, Ari B Hayes, Longfei Qiu, Yuwei Jin, Yanhao Chen, and Eddy Z Zhang. Time-optimal qubit mapping. In *Proceedings of the 26th ACM International Conference on Architectural Support for Programming Languages and Operating Systems*, pages 360–374, 2021.
- [43] Davide Venturelli, Minh Do, Eleanor Rieffel, and Jeremy Frank. Temporal planning for compilation of quantum approximate optimization circuits. In *Scheduling and Planning Applications workshop (SPARK)*, page 58, 2017.
- [44] Alwin Zulehner, Alexandru Paler, and Robert Wille. An efficient methodology for mapping quantum circuits to the ibm qx architectures.

IEEE Transactions on Computer-Aided Design of Integrated Circuits and Systems, 38(7):1226–1236, 2018.

- [45] Gushu Li, Yufei Ding, and Yuan Xie. Tackling the qubit mapping problem for nisq-era quantum devices. In *Proceedings of the Twenty-Fourth International Conference on Architectural Support for Programming Languages and Operating Systems*, pages 1001–1014, 2019.
- [46] Morten Kjaergaard, Mollie E Schwartz, Ami Greene, Gabriel O Samach, Andreas Bengtsson, Michael O’Keeffe, Christopher M McNally, Jochen Braumüller, David K Kim, Philip Krantz, et al. Programming a quantum computer with quantum instructions. *arXiv preprint arXiv:2001.08838*, 2020.
- [47] Jaeho Choi and Joongheon Kim. A tutorial on quantum approximate optimization algorithm (qaoa): Fundamentals and applications. In *2019 International Conference on Information and Communication Technology Convergence (ICTC)*, pages 138–142. IEEE, 2019.
- [48] J Robert Johansson, Paul D Nation, and Franco Nori. Qutip: An open-source python framework for the dynamics of open quantum systems. *Computer Physics Communications*, 183(8):1760–1772, 2012.



Tai-Ping Sun Tai-Ping Sun received the B.S. degree in Material Physics from University of Science and Technology of China, Hefei, China, in 2019. He is currently working toward the Ph.D. degree in Physics with the Department of Physics, University of Science and Technology of China, Hefei, China. His research interests include quantum computation, quantum machine learning and time series processing.



Bin-Han Lu Bin-Han Lu was born in Guangzhou, China, in 1997. He earned his Bachelor’s degree from Jinan University in 2019. Following that, he has been pursuing a Ph.D. at the CAS Center for Excellence in Quantum Information and Quantum Physics, University of Science and Technology of China, from 2019 to 2024. His research interests include quantum computing, quantum algorithms, and quantum hardware.



Peng Duan Peng Duan was born in Jiujiang, China, in 1993. He got his Bachelor’s degree from Shandong University in 2015 and his Ph.D. in physics from University of Science and Technology of China (USTC) in 2022. He is now a postdoctoral researcher at USTC. His main research interests focus on quantum computing and superconducting quantum devices.



Zhao-Yun Chen Zhao-Yun Chen was born in Wuhan, China, in 1994. He got his Bachelor’s degree from the University of Science and Technology of China (USTC) in 2016 and his Ph.D. in Physics from USTC in 2021. After that, he worked as a postdoctoral researcher at the Institute of Artificial Intelligence, Hefei Comprehensive National Science Center from 2021 to 2024. He then became an associate researcher there. His research interests include quantum computing, quantum algorithms, and quantum software.



Yu-Chun Wu Yu-Chun Wu, Ph.D., Assoc. Prof. Born in Qinghai, May 1974. Entered Shaanxi Normal University Math Dept. in 1991, graduated with a Master’s in 1998. Received a Ph.D. from the CAS Institute of Mathematics and Systems Science in 2001. Postdoc at USTC Quantum Information Lab from Jul 2001 to Feb 2004, stayed on as faculty. Additional postdoc at Gdansk University, Poland from Apr 2007 to Dec 2008. Research interests include quantum information theory, non-locality, entanglement, and quantum correlations.



Peng Wang Peng Wang received the B.S. degree in physics from Ocean University of China, Qingdao, China, in 2021. He is currently pursuing the Ph.D. degree at CAS Key Laboratory of Quantum Information, University of Science and Technology of China. His research interests include superconducting quantum computing, quantum algorithms, and quantum simulation.



Guo-Ping Guo Guo-Ping Guo, born in Nanchang, Jiangxi in December 1977, is a professor and doctoral supervisor. He is the leader in the research direction of semiconductor quantum dot quantum chips in the laboratory. He is the chief scientist of National Key Basic Research and Development Program Project Class A (Super 973) and a recipient of the National Distinguished Young Scholars Fund.



Huan-Yu Liu Huan-Yu Liu is from Fuyang, Anhui, China. He got his Bachelor’s degree from Hefei University of Technology in 2018 and his Ph.D. from the University of Science and Technology of China in 2023. He is currently engaged in postdoctoral research at the University of Science and Technology of China. His main research interests include quantum computing, quantum algorithms, and quantum simulation.